

Feasibility and Dosimetry Studies for ^{18}F -NOS as a Potential PET Radiopharmaceutical for Inducible Nitric Oxide Synthase in Humans

Pilar Herrero¹, Richard Laforest¹, Kooresh Shoghi¹, Dong Zhou¹, Gregory Ewald², John Pfeifer³, Eric Duncavage³, Kitty Krupp¹, Robert Mach¹, and Robert Gropler¹

¹Division of Radiological Sciences, Mallinckrodt Institute of Radiology, Washington University School of Medicine, St. Louis, Missouri; ²Cardiovascular Division, Department of Internal Medicine, Washington University School of Medicine, St. Louis, Missouri; and ³Division of Anatomic and Molecular Pathology, Department of Pathology and Immunology, Washington University School of Medicine, St. Louis, Missouri

Nitric oxide (NO), the end product of the inducible form of NO synthase (iNOS), is an important mediator of a variety of inflammatory diseases. Therefore, a radiolabeled iNOS radiopharmaceutical for assessing iNOS protein concentration as a marker for its activity would be of value to the study and treatment of NO-related diseases. We recently synthesized an ^{18}F -radiolabeled analog of the reversible NOS inhibitor, 2-amino-4-methylpyridine (^{18}F -NOS), and confirmed its utility in a murine model of lung inflammation. To determine its potential for use in humans, we measured ^{18}F -NOS myocardial activity in patients after orthotopic heart transplantation (OHT) and correlated it with pathologic allograft rejection, tissue iNOS levels, and calculated human radiation dosimetry. **Methods:** Two groups were studied—a kinetic analysis group and a dosimetry group. In the kinetic analysis group, 10 OHT patients underwent dynamic myocardial ^{18}F -NOS PET/CT, followed by endomyocardial biopsy. Myocardial ^{18}F -NOS PET was assessed using volume of distribution; standardized uptake values at 10 min; area under the myocardial moment curve (AUMC); and mean resident time at 5, 10, and 30 min after tracer injection. Tissue iNOS levels were measured by immunohistochemistry. In the dosimetry group, the biodistribution and radiation dosimetry were calculated using whole-body PET/CT in 4 healthy volunteers and 12 OHT patients. The combined time–activity curves were used for residence time calculation, and organ doses were calculated with OLINDA. **Results:** Both AUMC at 10 min ($P < 0.05$) and tissue iNOS ($P < 0.0001$) were higher in patients exhibiting rejection than in those without rejection. Moreover, the ^{18}F -NOS AUMC at 10 min correlated positively with tissue iNOS at 10 min ($R^2 = 0.42$, $P < 0.05$). ^{18}F -NOS activity was cleared by the hepatobiliary system. The critical organ was the bladder wall, with a dose of 95.3 $\mu\text{Gy}/\text{MBq}$, and an effective dose of 15.9 $\mu\text{Sv}/\text{MBq}$ was calculated. **Conclusion:** Myocardial ^{18}F -NOS activity is increased in organ rejection (a condition associated with increased iNOS levels) and correlates with tissue iNOS measurements with acceptable radiation exposure.

Although further modifications to improve the performance of ^{18}F -NOS are needed, these data show the feasibility of PET of iNOS in the heart and other tissues.

Key Words: cardiac; molecular imaging; positron emission tomography

J Nucl Med 2012; 53:1–8

DOI: 10.2967/jnumed.111.088518

Nitric oxide (NO) is an important and unique mediator of a variety of physiologic and pathologic processes (1,2). NO is generated from the oxidation of L-arginine to L-citrulline in a 2-step process by a nitric oxide synthase (NOS) family of enzymes (3). Three isoforms of NOS have been identified—2 constitutive isozymes, neuronal NOS (nNOS) and endothelial NOS (eNOS), and 1 inducible isozyme (iNOS). The 3 isozymes of NOS are expressed in different tissues to generate NO for specific physiologic roles. nNOS generates NO as a neurotransmitter and neuromodulator, mainly in the brain and peripheral nerve cells, and eNOS regulates blood pressure and blood flow, primarily in vascular endothelial cells (1). Whereas eNOS and nNOS are normal constituents of healthy cells, iNOS is not usually expressed. The increased production of NO by iNOS is implicated in a variety of acute and chronic inflammatory diseases such as sepsis, organ transplant rejection, vascular dysfunction in diabetes, asthma, arthritis, multiple sclerosis, and inflammatory diseases of the gut (4–7). Increased iNOS activity is also found in many tumors (8). Normally, the basal level of NO in all parts of the body is low, due mainly to the activity of nNOS and eNOS. In contrast, once expressed, iNOS can generate NO in large amounts (up to micromolar concentrations) for prolonged periods (1). Because of the central role of iNOS in the inflammatory component of disease, it is a target of intense efforts to develop novel therapeutics to control its activity (2,8–10). Thus, the availability of a noninvasive imaging approach to measure tissue iNOS levels would be highly desirable from

Received Jan. 26, 2011; revision accepted Jan. 24, 2012.

For correspondence or reprints contact: Robert J. Gropler, Cardiovascular Imaging Laboratory, Mallinckrodt Institute of Radiology, 510 S. Kingshighway Blvd., St. Louis, MO 63110.

E-mail: groplerr@mir.wustl.edu

Published online ■■■■

COPYRIGHT © 2012 by the Society of Nuclear Medicine, Inc.

both a clinical and a drug discovery or development perspective.

To this end, our group synthesized and evaluated several analogs of the reversible iNOS inhibitor 6-isopropyl-4-methylpyridin-2-amine and identified ^{18}F -6-(+/-)(2-fluoropropyl)-4-methylpyridin-2-amine (^{18}F -NOS) as a potential agent for imaging iNOS activity in vivo (11). This radiopharmaceutical demonstrated good selectivity for iNOS versus the other isoforms of the enzyme (approximately 6 and 2 times greater potency for inhibiting iNOS activity versus eNOS and nNOS activity, respectively) (11), in vitro stability, and high chemical and radiochemical purities. Moreover, in a murine model of lipopolysaccharide-induced pulmonary inflammation, compared with controls, ^{18}F -NOS lung activity was significantly increased and associated with increased iNOS protein levels (11). On the basis of these results, we sought to assess the potential of this radiopharmaceutical for imaging in humans. Accordingly, the current study had 2 goals. The first goal was to image increased iNOS protein levels in a human disease model known to exhibit elevated iNOS activity. To that end, we studied patients who had undergone orthotopic heart transplantation (OHT) and were under routine surveillance for allograft rejection by endomyocardial biopsy. These patients were chosen because iNOS activity is elevated in allograft rejection, and tissue is available for in vitro assay of iNOS protein levels (5,12). The second goal was to establish the normal biodistribution and calculate human radiation dosimetry of the radiopharmaceutical.

MATERIALS AND METHODS

^{18}F -NOS Synthesis

The proposed radiopharmaceutical, 6-(+/-)(2- ^{18}F -fluoropropyl)-4-methylpyridin-2-amine, was prepared from the (+/-) NOS-mesylate, the *N*-Boc-protected mesylated derivative of (+/-)NOS, by treatment with ^{18}F -KF/Kryptofix 222 (Merck), followed by deprotection with 1N HCl in accordance with a modified published procedure (11).

Human Subjects

Healthy volunteers ($n = 4$; 2 men and 2 women) were defined on the basis of a history and physical examination as having no acute or chronic diseases. Twenty-two OHT patients were studied. These patients were on standard immunosuppressive therapy and were undergoing routine surveillance for allograft rejection. The only exclusion criterion was the inability to tolerate 60–90 min of PET. The study consisted of 2 groups, a kinetic analysis group and a dosimetry group. The kinetic analysis group consisted of 10 OHT patients who underwent 60 min of dynamic imaging of the heart after administration of ^{18}F -NOS. In this group, the myocardial kinetics of the ^{18}F -NOS were compared with the clinical–pathologic diagnosis of allograft rejection and tissue iNOS protein levels measured on biopsy samples. In the dosimetry group, the 4 healthy volunteers and 12 additional OHT patients were imaged using a whole-body protocol for radiation dosimetry evaluation. In this group, endomyocardial biopsy was not performed for the OHT patients as part of the study. The protocol was performed under an exploratory investigational new drug application (106089) approved by the Food and Drug

Administration and by the Institutional Review Board at Washington University. Written informed consent was obtained from all subjects before enrollment into the study.

Patient Preparation and Protocol

All OHT subjects underwent routine clinical evaluation before the PET study as dictated by the treating transplant cardiologist. They were receiving standard immunosuppressive therapy and antihyperlipidemic, antihypertensive, and antidiabetic therapies as needed. Both the healthy volunteers and the OHT patients were studied after a light meal under resting conditions. The OHT patients took their prescribed medications on the day of the study. In the kinetic analysis group, the OHT patients underwent endomyocardial biopsy 3.3 ± 0.50 d after the PET/CT study. The endomyocardial biopsy was performed after imaging to exclude the potential confounding effects of myocardial inflammation after biopsy.

PET

PET images were acquired on a Biograph-40 TruePoint/TrueView PET/CT scanner (Siemens Medical Solutions Inc.).

Kinetic Analysis Protocol. Approximately 740 MBq of ^{15}O -water were administered intravenously, followed by a 5-min dynamic PET/CT data collection. Next, ^{18}F -NOS (~ 270 MBq) was administered intravenously, followed by 60 min of dynamic data acquisition. The ^{15}O -water images were used to localize the myocardium for coregistration of the ^{18}F -NOS images, which may not have adequate counting statistics for cardiac delineation. In addition, the measurements of myocardial blood flow from the ^{15}O -water datasets were to be used to assess the flow dependency of ^{18}F -NOS myocardial kinetics. Attenuation correction was provided by a low-dose spiral CT scan that covered the scanned area (120 kVp; 80 mAs effective; pitch, 0.8; collimation, 28.8 mm). The images were reconstructed on a 168×168 matrix with a 4.07-mm pixel size and 2-mm slice thickness and a 2-dimensional attenuation-weighted ordered-subset expectation maximization algorithm with 4 iterations and 8 subsets (13–15). Images were further processed with a postreconstruction 3-dimensional gaussian filter of 5 mm in full width at half maximum (FWHM).

^{15}O -water images (with correction for blood-pool activity based on the initial localization of activity in the left ventricle [LV]) encompassing the first 2 min of data and ^{18}F -NOS images encompassing the first 10 min of data were generated in the transaxial orientation. On each of these images, regions of interest (ROIs) were placed manually. On a mid-ventricular slice, a 3×3 voxel (~ 120 mm³) was placed in the center of the LV to obtain ^{15}O -water and ^{18}F -NOS vascular activity (MBq/mL). On this mid-ventricular slice and on immediately bordering slices, an anterior-lateral myocardial ROI (each ~ 6.0 cm³) was placed. Septal and inferior myocardial regions were excluded from the analysis because of contamination of ^{18}F -NOS activity emanating from the right ventricular cavity and liver, respectively (16). On the same slices, another 3 ROIs were placed on the pectoral muscle (used for graphical Logan analysis). Within these ROIs, myocardial blood flow was quantified on the basis of the ^{15}O -water kinetic data using a well-validated model (17). These ROIs were also transferred to the dynamic ^{18}F -NOS PET datasets to generate blood, myocardial, and pectoral muscle time–activity curves averaged and normalized by patient weight per injected dose (g/Bq). All curves were corrected for partial-volume effects on the basis of the knowledge of the LV

myocardial wall thickness measured on echocardiography and the performance characteristics of the scanner.

Several ^{18}F -NOS myocardial measurements were performed, including the distribution volume ratio (DVR), myocardial standardized uptake value (SUV) at 10 min, area under the moment curve (AUMC), and mean residence time (MRT) (18–20). Because of the rapid uptake and washout of the radiopharmaceutical in myocardium, AUMC and MRT measurements were performed at 5, 10, and 30 min after radiopharmaceutical administration. Details of these analytic methods can be found in the supplemental material (available online only at <http://jnm.snmjournals.org>).

Dosimetry Protocol. Healthy volunteers and OHT patients were injected with approximately 270 MBq of ^{18}F -NOS and imaged twice in the 4 h after injection. For each subject, the whole-body imaging protocol consisted of imaging at bed positions of 2–4 min each (based on patient size) to cover the whole torso (from head to mid thigh). Four groups of 4 subjects (1 healthy volunteer and 3 OHT patients) were imaged at the one of the following pairs of time points: 0 and 120 min, 30 and 150 min, 60 and 180 min, or 90 and 210 min. Combining the data from each group of subjects permitted the biodistribution of the radiopharmaceutical to be measured and its radiation dosimetry estimated using standard methods as detailed in the supplemental material (21,22).

Endomyocardial Biopsy, Clinical Pathologic, and iNOS Protein Measurements

Right ventricular endocardial biopsies were obtained percutaneously using standard clinical procedures and fixed in 4% formalin. Clinical–pathologic scoring of the biopsies was performed using the criteria of the International Society for Heart and Lung Transplantation (23). In brief, the categories of cellular rejection (R) ranged from grade 0 R (no rejection) to grade 3 R (severe rejection). A Quilty effect was added when mononuclear cell infiltrates were present. Immunohistochemistry of iNOS in tissue was performed using a modified biotin streptavidin alkaline phosphatase method as detailed in the supplemental material (5).

Statistical Analysis

Data are presented as mean value \pm SD. Two-sided unpaired *t* tests were used to compare between groups. Linear regression analysis was used to correlate quantitative PET measurement of ^{18}F -NOS DVR, AUMC, and MRT to the corresponding immunohistochemistry score. Regression coefficients and *P* values were calculated. A *P* value less than 0.05 was considered significant.

RESULTS

The clinical characteristics of the kinetic analysis and dosimetry groups are shown in Tables 1 and 2, respectively.

[Table 1] In the kinetic analysis group, there are equal numbers of men and women, with 5 patients being obese and 2 having diabetes. All patients exhibited normal left ventricular and right ventricular function based on the clinical report of the echocardiogram performed at the time of the endomyocardial biopsy. For the dosimetry group, 2 men and 2 women were classified as healthy volunteers. Of the 12 OHT patients, 3 were women and all but 1 had normal left ventricular and right ventricular function. At the time of the PET study, all patients were on a wide range of medications to prevent allograft rejection and to treat other comorbidities. No adverse events were observed during the PET study.

TABLE 1

OHT Patient Characteristics in PET Kinetic Analysis Cohort

Characteristic	Value
Sex (<i>n</i>)	
Male	5
Female	5
Mean age \pm SD (y)	46 \pm 9
Mean BMI \pm SD (kg/m ²)	28 \pm 12 (5 patients were obese, with BMI > 30)
Diabetes (<i>n</i>)	2
Range of left ventricular ejection fraction (%)	55–70
Right ventricular function	Normal
Time between transplantation and PET study (d)	
Mean \pm SD	409 \pm 367
Range	91–1,208
Time between PET and biopsy (d)	3.3 \pm 0.50

Kinetic Analysis Study

Shown in Figure 1 are the myocardial PET/CT images **[Fig. 1]** and iNOS scores from 4 patients with various levels of allograft rejection based on the clinical pathology report. Shown in Figure 2 are the myocardial time–activity curves **[Fig. 2]** expressed in SUV scale for 2 of the patients with and without rejection. On average, those patients exhibiting rejection had significantly higher levels of iNOS staining and values for AUMC at 10 min than did patients without rejection (Fig. 3). No significant differences were noted between patients with and without rejection for AUMC at 5 or 30 min; MRT at 5, 10, or 30 min; SUV; or DVR (data not **[Fig. 3]**

TABLE 2

Patient Characteristics in PET Dosimetry Cohort

Characteristic	Value
Healthy volunteers (<i>n</i> = 4)	
Sex (<i>n</i>)	
Male	2
Female	2
Mean age \pm SD (y)	30 \pm 11
Mean BMI \pm SD (kg/m ²)	26 \pm 5
OHT patients (<i>n</i> = 12)	
Sex	
Male	9
Female	3
Mean age \pm SD (y)	52 \pm 12
Mean BMI \pm SD (kg/m ²)	27 \pm 5 (obese = 2; BMI > 30)
Range of left ventricular ejection fraction (%)	55–70: 11/12
	<55: 1/12
Right ventricular function	Normal
Time between transplantation and PET study (d)	
Mean \pm SD	1,783 \pm 1,191
Range	152–3,663

shown). Moreover, the level of myocardial blood flow did not differ between the patient with and the patient without clinical–pathologic evidence of rejection (Fig. 3).

[Table 3] Shown in Table 3 are individual values for iNOS staining, AUMC, MRT, SUV, and DVR at 10 min. Only AUMC at 10 min correlated significantly, albeit weakly, with iNOS staining ($R^2 = 0.40$, $P < 0.05$). No significant correlation with iNOS staining was noted for DVR or SUV (at 10 min) (data not shown). Moreover, no correlation was observed with tissue iNOS for AUMC at 5 or 10 min and MRT at 5, 10, or 30 min (Supplemental Figs. 1 and 2). Neither AUMC at 10 min nor iNOS score correlated with myocardial blood flow (Fig. 4), suggesting that kinetic measures of iNOS activity were not influenced by blood flow.

Dosimetry Study

Biodistribution Data and Time–Activity Curves. In the dosimetry group, accumulation was seen mostly in the urinary bladder (excretion) and to a varying degree in the gallbladder and stomach. Typical whole-body images are presented in Figure 5. Activity was also seen to accumulate in the liver and kidneys and then transit to the urethras and bladder. The spleen could be observed at early time points because of its large blood content. Little activity was observed in the brain, and the activity was not specific to any cerebral structure. No activity was observed to accumulate in the intestines (apart from blood) during the imaging time. Also, as seen in Figure 5, substantial activity appears to be distributed uniformly and nonspecifically to the soft tissues.

Time–activity curves for the various organs are presented in the supplemental material (Supplemental Figs. 3A–3H), along with the monoexponential fits. The monoexponential function is seen to represent the data well for most organs. The gallbladder is observed to increase linearly over time and is observed to have high large interpatient fluctuations, most likely due to the fat content of the diet, which was unknown. Therefore, activity in this organ is associated with its content.

[Table 4] Activity residence times are presented in Table 4. Cumulative activity in the urinary bladder was used to create the urine time–activity curve. This curve was then fitted with an uptake function to extract the average filling fraction and

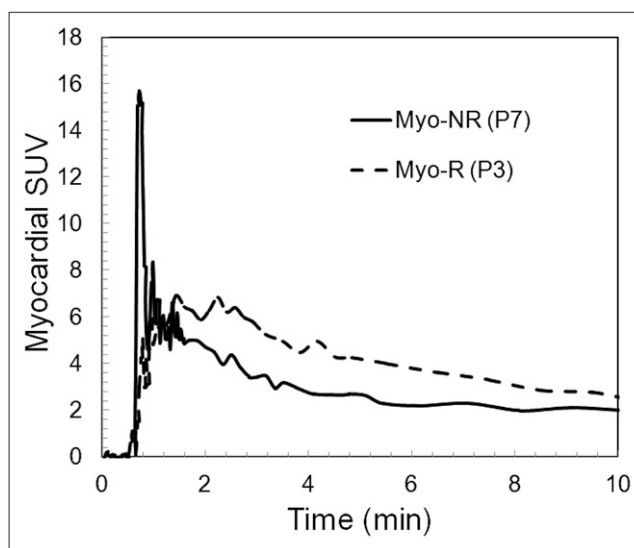


FIGURE 2. Myocardial ^{18}F -NOS time–activity curves for patients 7 (P7) and 3 (P3) shown in Figure 1. Curves demonstrate rapid turnover of ^{18}F -NOS in tissue and greater uptake with rejection. Myo = myocardial; NR = no rejection; R = rejection.

the filling time. The MIRD bladder excretion mode was then used with a voiding period of 1 h (21). Activity in the blood was measured by PET in a left ventricular ROI. The blood residence time was also assigned to the remainder of the body. The errors in the residence time were calculated from the $1-\sigma$ uncertainties of the parameter estimates. These error estimates were primarily determined by interpatient fluctuations. Sixteen percent of the activity was measured in the various organs as visible on the images, 13% was excreted in the urine (1-h void model), and 71% was assigned nonspecifically to the remainder of the body. The blood activity concentration from an ROI placed in the LV is plotted in Supplemental Figure 4. The data were obtained by assuming an 8% blood volume per body weight and was fitted with a double-exponential function. The biologic half-life for ^{18}F -NOS in the blood was 126 min.

Radiation Doses. Organ radiation doses were calculated with the MIRD approach using the OLINDA/EXM software (version 1.1), the standard adult male model, and the residence times as previously calculated. Organ radiation doses, along with their error estimates, are summarized in Table 5. The error estimates are propagated from the uncertainties of organ residence times. The organ receiving the highest dose was the urinary bladder wall, with a dose of $95.3 \mu\text{Gy}/\text{MBq}$, followed by the gallbladder wall at $25.6 \mu\text{Gy}/\text{MBq}$. The effective dose was $15.9 \mu\text{Sv}/\text{MBq}$.

DISCUSSION

In this study, we evaluated the feasibility of ^{18}F -NOS, a newly synthesized PET radiopharmaceutical, to assess myocardial iNOS levels in patients who have undergone cardiac transplantation. Both tissue iNOS protein levels and the myocardial AUMC for ^{18}F -NOS at 10 min after

RGB

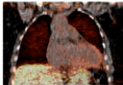
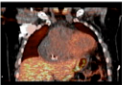

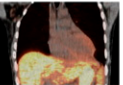
Patient	P7	P3	P6	P10
PET/CT				
Rejection score	NR	R1QE	R1	R1QE
iNOS score	41.99	157.41	136.41	131.39

FIGURE 1. Myocardial ^{18}F -NOS PET/CT images from 1 to 10 min after injection in 4 OHT patients, with corresponding allograft rejection (R) grades based on clinical pathology report and immunohistochemistry-derived iNOS score. NR = no rejection; QE = Quilty effect, which is associated with acute cellular rejection.

[Table 5]

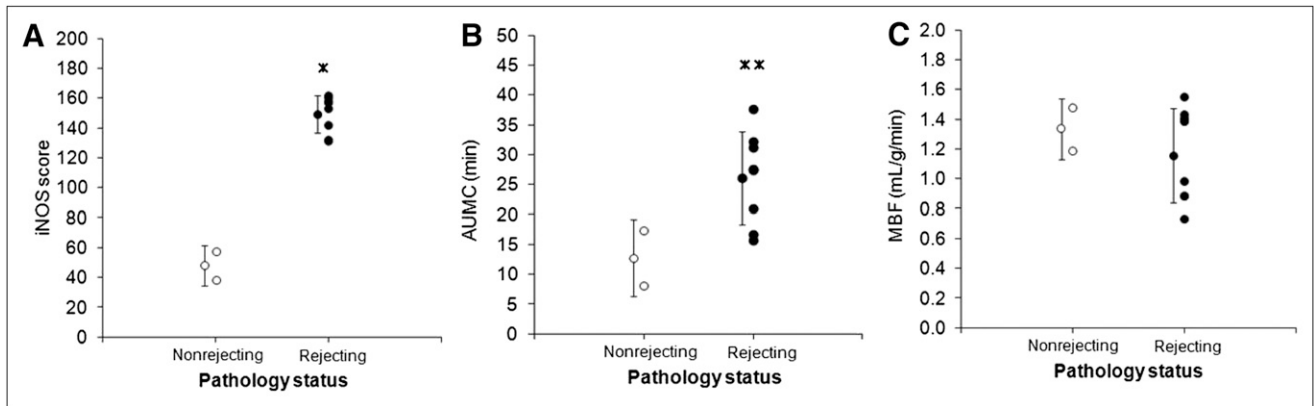


FIGURE 3. iNOS score (A), myocardial ^{18}F -NOS AUMC at 10 min (B), and myocardial blood flow (C) in patients with and without rejection based on clinical pathology report. * $P < 0.0001$. ** $P < 0.05$.

injection were significantly higher in patients exhibiting allograft rejection than in patients without rejection, consistent with the central role of iNOS in this pathologic process. Moreover, the AUMC values at 10 min correlated directly with tissue iNOS levels. We also confirmed that these measurements could be obtained with acceptable radiation exposure. Biodistribution imaging indicated that elimination of ^{18}F -NOS was primarily by the hepatobiliary system, with substantial accumulation in the urinary bladder. Radiation dosimetry estimates showed that both the highest organ dose (the urinary bladder wall) and the effective dose were comparable to those reported for ^{18}F -FDG.

Correlation of Myocardial ^{18}F -NOS Kinetics and Tissue iNOS Levels

In a mouse model of lipopolysaccharide-induced iNOS activation, higher uptake of ^{18}F -NOS in the lungs was observed for the lipopolysaccharide-treated mice than for the control mice, and this difference correlated well with iNOS expression (11). These data suggested that ^{18}F -NOS may be a useful radiopharmaceutical to assess tissue iNOS levels with PET. In the current study, we performed myocardial imaging in OHT patients undergoing surveillance for allograft rejection because this patient population provided the twin advantages of likely increases in cellular iNOS levels and the ability to correlate the PET measurements with tissue assay of iNOS protein. By using the exploratory investigational new drug application mechanism in OHT patients, we were able to shorten the translational timeline to assess the feasibility of this radiopharmaceutical for human imaging.

The myocardial time-activity curves indicated rapid radiopharmaceutical uptake and clearance. This pattern is consistent with a reversibly bound process but different from what we observed in a mouse lung injury model where radiopharmaceutical uptake was still present at 60 min (11). These differences may well reflect the combined effects of species and organ differences in radiopharmaceutical kinetics and in the magnitude of iNOS activation between the 2 studies. To assess the feasibility of ^{18}F -NOS, we characterized several PET measurements including DVR, SUV,

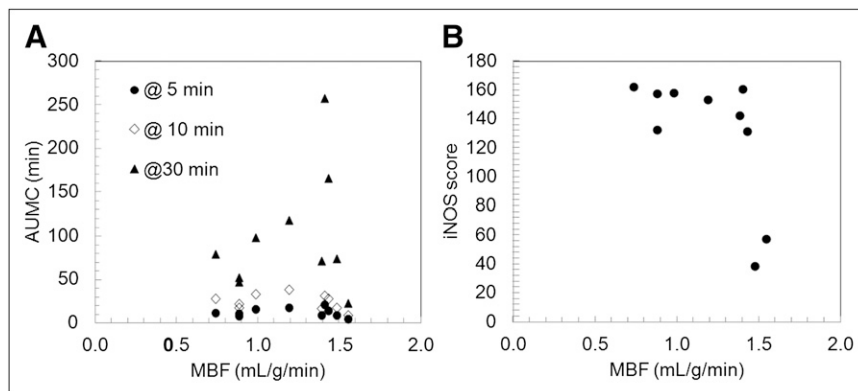
MRT, and AUMC. The SUV at 10 min did not correlate with tissue iNOS measurements, most likely because of potential intersubject variability in ^{18}F -NOS metabolism and the presence of radiolabeled metabolites in tissue. Myocardial activity of ^{18}F -NOS—a radiopharmaceutical with reversible binding kinetics—was determined by measuring DVR using the Logan plot analysis (18). However, ^{18}F -NOS DVR was not correlated with tissue iNOS measurements. We performed the Logan analysis using a reference region (pectoral muscle). The application of Logan analysis using a reference region assumes that there is no uptake of radiopharmaceutical in the reference region. In addition, such an analysis requires a priori knowledge of the clearance constants for proper calculation of DVR. Because obese individuals may have some degree of systemic inflammation leading to increased iNOS levels in the pectoral muscle, some binding may have occurred in the reference region (24). In addition, in the absence of a radiolabeled metabolite-corrected input function, we could not obtain estimates of the clearance phase for proper application of Logan analysis. In a similar vein, we did not observe a correlation between tissue iNOS protein levels and ^{18}F -NOS MRT measurements at any time point used or between

TABLE 3
Individual Data for Tissue iNOS Score and PET

Patient no.	iNOS score	AUMC (min)	MRT (min)	SUV	DVR
1	160.40	31.2	4.47	4.40	1.35
2	161.83	27.4	5.22	3.38	0.99
3	157.93	32.2	4.07	10.23	0.97
4	157.41	16.7	4.66	7.09	0.83
5	132.16	20.9	5.41	4.25	1.07
6	152.91	37.6	4.14	2.85	0.72
7	57.30	8.2	4.61	7.54	3.55
8	38.24	17.3	4.66	4.93	1.71
9	142.19	15.7	4.57	2.57	0.92
10	131.39	27.6	5.02	6.31	0.90

All PET data are at 10 min after injection of ^{18}F -NOS.

FIGURE 4. ^{18}F -NOS AUMC at 5, 10, and 30 min (A) and immunochemistry-derived iNOS score (B) plotted as function of myocardial blood flow (MBF) derived from ^{15}O -water studies.



tissue iNOS protein levels and AUMC at 5 or 30 min. The presence of a significant correlation between PET ^{18}F -NOS and AUMC at 10 min (Fig. 4) likely was the result of less impact of these variables at this time point. To assess whether kinetic measures, in particular AUMC at 10 min, were influenced by blood flow, we correlated PET measures of iNOS activity to blood flow. There was no correlation between myocardial blood flow and AUMC or tissue iNOS levels, suggesting that the observed correlations were not a flow-related phenomenon.

The observed variability in image-derived iNOS measures, and the lack of correlation in some instances between PET ^{18}F -NOS measures and biopsy iNOS measurements, can be attributed to several other factors as well. First, ^{18}F -NOS was sampled from anterolateral myocardium, whereas iNOS was sampled from the right ventricular endomyocardial interventricular septal wall, resulting in interrogation of different parts of the myocardium. Second, PET/CT scanners have relatively low resolution when compared with the cellular histochemistry method used as a gold standard for endomyocardial iNOS measurements, precluding clear delineation of endocardium sampling. Third, the heterogeneous distribution of inflammation on the biopsy samples can lead to over- or undersampling on immunohistochemistry. Fourth, the presence of radiolabeled metabolites may

confound the interpretation of the PET signal. Five, although ^{18}F -NOS does have higher selectivity for iNOS than eNOS and nNOS, the magnitudes of the differences are relatively modest at 6 \times and 2 \times , respectively. Thus, measured activity may represent the contribution from eNOS and nNOS. However, in most conditions in which iNOS expression is increased, levels of NO production are many orders of magnitude higher than those produced by eNOS or nNOS, because only iNOS is under transcriptional control. Thus, ^{18}F -NOS activity would reflect primarily iNOS activity. That being said, these assumptions need to be validated by further studies on conditions in which eNOS or nNOS activity is increased in conjunction with iNOS activity, such as in ischemia–reperfusion injury, various tumors, and Alzheimer disease (25–27). Finally, PET with ^{18}F -NOS is measuring iNOS protein emanating from all cell types (e.g., myocytes or macrophages) within the myocardial ROI. Given the low spatial resolution of PET, the technique cannot identify the relative contribution of signal from these sources. That being said, PET with ^{18}F -NOS provides a non-invasive integrated measure of iNOS protein levels within the human heart that heretofore has not been possible.

Taken in sum, these data suggest that the myocardial kinetics of ^{18}F -NOS tracks with histologic measures of iNOS independent of blood flow, providing evidence that PET of



FIGURE 5. Typical ^{18}F -NOS whole-body PET images for 2 patients: first patient imaged at 0 and 120 min and second patient imaged at 90 and 150 min after injection.

TABLE 4
Organ Residence Times

Organ	Residence time (h)
Liver	0.148 ± 0.016
Spleen	0.011 ± 0.004
Kidneys	0.028 ± 0.007
Brain	0.021 ± 0.006
Heart wall	0.010 ± 0.004
Stomach	0.006 ± 0.003
Gallbladder	0.008 ± 0.004
Urinary bladder	0.18 ± 0.04
Excreted	0.33 ± 0.07
Remainder of body	1.88 ± 0.40

Bladder residence time was calculated using MIRD bladder-voiding model with cumulative activity and voiding period of 1 h.

iNOS may be possible in humans. However, the rapid washout of the radiopharmaceutical in myocardium, at this stage, appears to limit its imaging capability. The fast washout kinetics of ¹⁸F-NOS is related to the unfavorable potency for inhibiting iNOS activity (inhibitory concentration of 50%, 220 nM). Accordingly, future efforts in our laboratory are focused on developing new radiolabeled iNOS inhibitors based on known compounds having a higher potency for inhibiting iNOS than 6-isopropyl-4-methylpyridin-2-amine, the lead compound used in our current studies (11). A PET radiotracer having a greater potency for inhibiting iNOS than that of ¹⁸F-NOS should display a slower rate of washout of activity from target tissue.

Biodistribution and Radiation Dosimetry of ¹⁸F-NOS

The PET biodistribution images indicated an elimination of the tracer by the hepatobiliary system (average of 23%), with substantial accumulation in the bladder- (filling time of 20 min). Clearance from the blood was measured with a biologic half-life of approximately 2 h, suggesting rapid metabolism and slow clearance. Further analysis will be required to determine whether the circulation activity is in the form of the native ¹⁸F-NOS compound or in the form of metabolites. Significant accumulation of the tracer is also visible in the gallbladder, in which it was observed that activity accumulates over time. The clearance of activity is well explained by a simple monoexponential function for most organs, with an average biologic half-life of approximately 80 min for organs and 120 min for the blood. The organ receiving the highest dose was the urinary bladder wall, at 95.3 μGy/MBq, followed by the gallbladder wall, at 25.6 μGy/MBq. For the present calculation, we have assumed a voiding interval of 1 h, and in this condition the bladder wall is still the dose-limiting organ. The ¹⁸F-NOS effective dose was 15.9 μSv/MBq. For a maximum allowed radiation dose to any organ of 50 mSv in a single study as prescribed by the Code of Federal Regulation, the permissible injected dose is 525 MBq (14.2 mCi), and the effective dose is 9.87 mSv (0.987 rem). These doses are comparable to the dose

delivered to the bladder wall and the effective dose from ¹⁸F-FDG, at 160 μGy/MBq and 19 μSv/MBq, respectively (28).

CONCLUSION

We have shown the feasibility in humans of measuring myocardial iNOS levels with PET and ¹⁸F-NOS with acceptable biodistribution and radiation exposure. Further optimization of the radiopharmaceutical to slow its washout from tissue and more evaluation to fully characterize its metabolism and its kinetics through appropriate mathematic schemes are needed. That being said, these studies showcase the feasibility of measuring of iNOS levels in the heart and other tissues with PET. Given the central role of iNOS in a variety of disease processes, PET may provide new avenues for the clinical management of these patients and facilitate the drug discovery or development process for new therapies that target iNOS activity.

DISCLOSURE STATEMENT

The costs of publication of this article were defrayed in part by the payment of page charges. Therefore, and solely to indicate this fact, this article is hereby marked “advertisement” in accordance with 18 USC section 1734.

TABLE 5
Organ Radiation Doses

Organ	Dose
Adrenals	12.1 ± 2.4
Brain	5.5 ± 2.3
Breasts	8.0 ± 1.4
Gallbladder	25.6 ± 15
Lower large intestine wall	13.4 ± 3.0
Small intestine	12.5 ± 2.4
Stomach wall	12.7 ± 4.2
Upper large intestine wall	12.3 ± 2.6
Heart wall	12.6 ± 5.7
Kidneys	23.4 ± 10.0
Liver	22.5 ± 5.0
Lungs	9.8 ± 1.8
Muscle	10.0 ± 1.9
Ovaries	13.6 ± 3.0
Pancreas	12.7 ± 3.0
Red marrow	10.2 ± 2.1
Osteogenic cells	15.1 ± 2.6
Skin	7.6 ± 1.4
Spleen	17.1 ± 9.6
Testes	10.7 ± 2.2
Thymus	9.8 ± 1.8
Thyroid	9.5 ± 1.6
Urinary bladder wall	95.3 ± 39.8
Uterus	16.7 ± 4.4
Total body	10.4 ± 2.0
Effective dose equivalent*	18.8 ± 6.2
Effective dose*	15.9 ± 4.6

*All radiation doses are in μGy/MBq except for effective dose and effective dose equivalent, which are in μSv/MBq.

ACKNOWLEDGMENTS

This work was supported by NIH/NHLBI 5P01-HL-13851. No other potential conflict of interest relevant to this article was reported.

REFERENCES

1. Alderton WK, Cooper CE, Knowles RG. Nitric oxide synthases: structure, function and inhibition. *Biochem J*. 2001;357:593–615.
2. Mollace V, Muscoli C, Masini E, Cuzzocrea S, Salvemini D. Modulation of prostaglandin biosynthesis by nitric oxide and nitric oxide donors. *Pharmacol Rev*. 2005;57:217–252.
3. Marletta MA. Nitric oxide synthase structure and mechanism. *J Biol Chem*. 1993;268:12231–12234.
4. Kaneki M, Shimizu N, Yamada D, Chang K. Nitrosative stress and pathogenesis of insulin resistance. *Antioxid Redox Signal*. 2007;9:319–329.
5. Koch A, Burgschweiger A, Herpel E, et al. Inducible NO synthase expression in endomyocardial biopsies after heart transplantation in relation to the postoperative course. *Eur J Cardiothorac Surg*. 2007;32:639–643.
6. Lechner M, Lirk P, Rieder J. Inducible nitric oxide synthase (iNOS) in tumor biology: The two sides of the same coin. *Semin Cancer Biol*. 2005;15:277–289.
7. Smith KJ, Lassmann H. The role of nitric oxide in multiple sclerosis. *Lancet Neurol*. 2002;1:232–241.
8. Fitzpatrick B, Mehibel M, Cowen RL, Stratford IJ. iNOS as a therapeutic target for treatment of human tumors. *Nitric Oxide*. 2008;19:217–224.
9. McCarthy HO, Coulter JA, Robson T, Hirst DG. Gene therapy via inducible nitric oxide synthase: a tool for the treatment of a diverse range of pathological conditions. *J Pharm Pharmacol*. 2008;60:999–1017.
10. Pannu R, Singh I. Pharmacological strategies for the regulation of inducible nitric oxide synthase: Neurodegenerative versus neuroprotective mechanisms. *Neurochem Int*. 2006;49:170–182.
11. Zhou D, Lee H, Rothfuss JM, et al. Design and synthesis of 2-amino-4-methylpyridine analogues as inhibitors for inducible nitric oxide synthase and in vivo evaluation of [¹⁸F]6-(2-fluoropropyl)-4-methyl-pyridin-2-amine as a potential PET tracer for inducible nitric oxide synthase. *J Med Chem*. 2009;52:2443–2453.
12. Lewis NP, Tsao PS, Rickenbacher PR, et al. Induction of nitric oxide synthase in the human cardiac allograft is associated with contractile dysfunction of the left ventricle. *Circulation*. 1996;93:720–729.
13. Comtat C, Kinahan PE, Defrise M, Michel C, Townsend DW. Fast reconstruction of 3D-PET data with accurate statistical modeling. *IEEE Trans Nucl Sci*. 1998;45:1083–1089.
14. Hebert T, Leahy RM. Fast methods for including attenuation correction in the EM algorithm. *IEEE Trans Nucl Sci*. 1990;37:754–758.
15. Hudson HM, Larkin LS. Accelerated image reconstruction using ordered subsets of projection data. *IEEE Trans Med Imaging*. 1994;13:601–609.
16. Gropler RJ, Siegel BA, Sampathkumaran K, et al. Dependence of recovery of contractile function on maintenance of oxidative metabolism after myocardial infarction. *J Am Coll Cardiol*. 1992;19:989–997.
17. Bergmann SR, Herrero P, Markham J, Weinheimer CJ, Walsh MN. Noninvasive quantitation of myocardial blood flow in human subjects with oxygen-15-labeled water and positron emission tomography. *J Am Coll Cardiol*. 1989;14:639–652.
18. Logan J, Fowler JS, Volkow ND, Wang GJ, Ding YS, Alexoff DL. Distribution volume ratios without blood sampling from graphical analysis of PET data. *J Cereb Blood Flow Metab*. 1996;16:834–840.
19. Bailer AJ. Testing for the equality of area under the curves when using destructive measurement techniques. *J Pharmacokinetic Biopharm*. 1988;16:303–309.
20. Weiss M. The relevance of residence time theory to pharmacokinetics. *Eur J Clin Pharmacol*. 1992;43:571–579.
21. Thomas SR, Stabin MG, Chen CT, Samarutunga RC. MIRD pamphlet no. 14 revised: a dynamic urinary bladder model for radiation dose calculations. *J Nucl Med*. 1999;40:102S–123S.
22. Stabin MG, Sparks RB, Crowe E. OLINDA/EXM: The Second-Generation Personal Computer Software for Internal Dose Assessment in Nuclear Medicine. *J Nucl Med*. 2005;46:1023–1027.
23. Stewart S, Winters GL, Fishbein MC, et al. Revision of the 1990 Working Formulation for the Standardization of Nomenclature in the Diagnosis of Heart Rejection. *J Heart Lung Transplant*. 2005;24:1710–1720.
24. Shoelson SE, Herrero L, Naaz A. Obesity, inflammation, and insulin resistance. *Gastroenterology*. 2007;132:2169–2180.
25. Bolli R. Cardioprotective function of inducible nitric oxide synthase and role of nitric oxide in myocardial ischemia and preconditioning: an overview of a decade of research. *J Mol Cell Cardiol*. 2001;33:1897–1918.
26. Fukumura D, Kashiwagi S, Jain RK. The role of nitric oxide in tumour progression. *Nat Rev Cancer*. 2006;6:521–534.
27. Lüth HJ, Holzer M, Gärtner U, Staufenbiel M, Arendt T. Expression of endothelial and inducible NOS-isoforms is increased in Alzheimer's disease, in APP23 transgenic mice and after experimental brain lesion in rat: evidence for an induction by amyloid pathology. *Brain Res*. 2001;913:57–67.
28. International Commission on Radiological Protection (ICRP). *Radiation Dose to Patients from Radiopharmaceuticals: ICRP Publication 80, in Addendum to ICRP Publication 53*. Oxford U.K.: Pergamon Press; 1999.